PHYSICS OF FLUIDS **26**, 111901 (2014)

Gyrotactic trapping in laminar and turbulent Kolmogorov flow

Francesco Santamaria,[1] Filippo De Lillo,[1] Massimo Cencini,[2,a)] and Guido Boffetta[1]
[1]*Dipartimento di Fisica and INFN, Università di Torino, via P. Giuria 1, 10125 Torino, Italy*
[2]*Istituto dei Sistemi Complessi, CNR, via dei Taurini 19, 00185 Rome, Italy*

(Received 15 July 2014; accepted 10 October 2014; published online 6 November 2014)

Phytoplankton patchiness, namely the heterogeneous distribution of microalgae over multiple spatial scales, dramatically impacts marine ecology. A spectacular example of such heterogeneity occurs in thin phytoplankton layers (TPLs), where large numbers of photosynthetic microorganisms are found within a small depth interval. Some species of motile phytoplankton can form TPLs by gyrotactic trapping due to the interplay of their particular swimming style (directed motion biased against gravity) and the transport by a flow with shear along the direction of gravity. Here we consider gyrotactic swimmers in numerical simulations of the Kolmogorov shear flow, both in laminar and turbulent regimes. In the laminar case, we show that the swimmer motion is integrable and the formation of TPLs can be fully characterized by means of dynamical systems tools. We then study the effects of rotational Brownian motion or turbulent fluctuations (appearing when the Reynolds number is large enough) on TPLs. In both cases, we show that TPLs become transient, and we characterize their persistence. © *2014 AIP Publishing LLC*. [http://dx.doi.org/10.1063/1.4900956]

I. INTRODUCTION

Motile aquatic microorganisms in their natural habitats move under the simultaneous and combined effect of ambient transport (currents, turbulence, etc.) and swimming.[1,2] The interaction between these different transport mechanisms can give rise to interesting phenomena, such as the generation of inhomogeneous distributions[3,4] and swimming-induced flows like bioconvection[5,6] or bacterial turbulence,[7] many aspects of which can be studied within the theoretical framework of dynamical systems theory and fluid mechanics.[8–14]

For most microorganisms, swimming is biased in specific directions by some kind of *taxis* in response to chemical (e.g., *chemotaxis*[15]) or physical signals (e.g., *phototaxis*[16] and *magnetotaxis*[17]). One of those taxes, relevant to several species of phytoplankton, tends to orient cell swimming direction upward against gravity (negative *gravitaxis*). Although other mechanisms are also possible, vertical orientation typically results from the gravitational torque due to the asymmetric cell-density distribution leading to bottom heaviness.[1–3] In the presence of a flow, gravitational torque combines with the hydrodynamic one giving rise to directed locomotion, dubbed *gyrotaxis*, which can eventually cause accumulation of cells in specific flow regions. In a laminar downwelling pipe flow, for instance, the interplay of swimming and hydrodynamic shear produces a striking aggregation in the center of the pipe known as gyrotactic focusing.[3] In homogeneous isotropic turbulence, numerical simulations have shown that gyrotactic algae generate small-scale clusters with fractal distributions.[13,14] Such findings, which have been rationalized using tools from dynamical systems and fluid mechanics, may be an explanation of why field observations have found that small-scale patchiness appears to be stronger in motile phytoplankton species.[18–20]

[a)]Author to whom correspondence should be addressed. Electronic mail: massimo.cencini@cnr.it

In this paper, we consider a case intermediate between laminar flows and homogeneous turbulence: turbulence in the presence of a mean shear flow. The motivation for our study comes from the recent experimental observation that gyrotactic algae swimming within a laminar vertical shear aggregate in horizontal layers around the maximal shear rate, as a consequence of *gyrotactic trapping*.[4] This mechanism has been proposed as a possible explanation, at least for some phytoplankton species, for the formation of the spectacular thin phytoplankton layers (TPLs) often observed in (coastal) ocean. TPLs are high concentrations of phytoplankton, centimeters to 1 m thick, which extend horizontally up to kilometers and last from hours to a few days.[21–25] They are important to marine ecology by enhancing zooplankton growth rates, thus providing high concentration of preys for fishes and their larvae. Moreover, as many phytoplankton species found in TPLs are toxic, their presence can enhance zooplankton and fish mortality, or induce zooplankton to avoid toxic and mucus rich layers. TPLs can be formed by several motile and non-motile species, therefore very likely there is not a unique mechanism for their formation. See the review of Ref. 25 and references therein for an up-to-date account on various aspects of TPLs.

It is worth recalling the basic ideas of the microfluidic experiments,[4] which have demonstrated gyrotactic trapping for *Chlamydomonas nivalis* and *Heterosigma akashiwo* (a toxic species). Swimming algae were injected at the bottom of a centimeter-sized tank where a vertical shear is induced by a rotating belt. Cells swim upwards to about the middle of the tank where the shear rate becomes sufficiently strong to overcome gravitational bias and cause the swimming direction to tumble. Loosing gravitational bias, no net vertical velocity can be maintained. Hence, cells remain trapped, accumulating in horizontal layers. Recent numerical simulations have shown that gyrotactic phytoplankton forms thin layers even in non-stationary Kelvin-Helmholtz (KH) flow, where swimming cells are found to be trapped in evolving KH billows.[26] However, field experiments with simultaneous measurement of biological and physical properties have shown that while thin layers are weakly affected by turbulence of moderate intensity, stronger turbulence will dissolve them.[27,28] The entire process is rather nontrivial and poorly understood:[25] on the one hand shear flows can induce layers by gyrotactic trapping; on the other hand they trigger the generation of turbulence which, in turn, can destabilize gyrotactic trapping causing layers' break-up.

In the present paper, we study phytoplankton layers in the Kolmogorov flow with shear along the vertical direction. This is a well-known periodic shear flow model for studying the transition to turbulence[29–31] and it is presented together with the model equations for gyrotactic motion in Sec. II.

In laminar and steady Kolmogorov flow (Sec. III), we have been able to solve gyrotactic swimmer dynamics by using tools from dynamical systems. In particular, we have found that the motion is integrable, allowing us to analytically characterize gyrotactic trapping. We have then numerically studied the effect of stochasticity, namely, rotational Brownian motion, on the evolution of the thin layers (Sec. IV).

In the turbulent Kolmogorov flow, small-scale fluctuations superimpose to the mean large scale flow, and no analytical study is possible. Direct numerical simulations of the Navier-Stokes equations, coupled with the Lagrangian dynamics of gyrotactic swimmers, have been used to investigate the dynamical effects of turbulent fluctuations on TPLs (Sec. V).

Both stochastic effects and turbulence make TPL a transient phenomenon, and we characterized its persistence properties. Discussions and final remarks on the relevance of our findings are presented in Sec. VI.

II. MODELS

A. Gyrotactic swimming

We consider spherical cells, which is justified by detailed analysis of cell morphology,[32] and dilute suspensions so that alga-alga interactions can be neglected as well as back-reaction on the fluid flow. Moreover, thanks to the small size of the cells ($\sim 10\,\mu$m) with respect to the Kolmogorov length scale (η, namely, the smallest scale of turbulent flows, in oceans $\eta \sim 0.3-10$ mm) they can be considered as point particles and their motion is akin to that of passive tracers but for their ability

to swim. We assume that cells are neutrally buoyant, as their sedimentation speed ($\sim 2.5-3\,\mu$m/s) is much smaller than their typical swimming speed ($\sim 100\,\mu$m/s).[5,32]

According to the classic model of gyrotactic motility,[1–3] the position $\boldsymbol{X}$ and the swimming orientation $\mathbf{p}$ (where $|\mathbf{p}| = 1$) of a gyrotactic cell evolve according to the equations

$$\dot{\boldsymbol{X}} = \boldsymbol{u} + v_s \mathbf{p}\,, \tag{1}$$

$$\dot{\mathbf{p}} = \frac{1}{2B}\left[\hat{z} - (\hat{z}\cdot\mathbf{p})\mathbf{p}\right] + \frac{1}{2}\boldsymbol{\omega}\times\mathbf{p}\,, \tag{2}$$

$\hat{z}$ denoting the vertical unit vector. In Eq. (1), the cell velocity is given by the superposition of the fluid velocity at the cell location, $\boldsymbol{u}(\boldsymbol{X}, t)$, and the swimming velocity, $v_s\mathbf{p}$, with v_s assumed to be constant.[1,2] As for the swimming direction dynamics, the first term on the r.h.s. of Eq. (2) accounts for the bias in the direction opposite to gravitational acceleration, $\boldsymbol{g} = -g\hat{z}$, with a characteristic orientation time B (in a still fluid, $\boldsymbol{u} = 0$, B is the typical time a cell employs to orient upwards). For bottom-heavy, neutrally buoyant, and spherical cells in a fluid with kinematic viscosity ν we have $B = 3\nu/(hg)$, h measuring the distance between the cell center of mass and its geometric center. We remark that this term has, in general, an additional contribution arising from fluid acceleration.[14] However for the formation of TPLs in the oceans, where turbulence is not very intense, with typical values of the turbulent energy dissipation $\epsilon \ll 10^{-4}\text{m/s}^3$ (see, e.g., Ref. 33), fluid acceleration ($\sim(\epsilon^3/\nu)^{1/4} \approx 0.1\,\text{m/s}^2 \ll g$) can be safely neglected. Finally, the last term in (2) represents the rotation of the swimming direction due to fluid vorticity $\boldsymbol{\omega} = \boldsymbol{\nabla}\times\boldsymbol{u}$.

By comparing the two terms in Eq. (1), we can define the *swimming number* $\Phi = v_S/U$ where U is a typical velocity of the flow, providing a dimensionless measure of the swimming velocity. While from Eq. (2) we obtain the dimensionless *stability number* $\Psi = B\omega$, where ω is a measure of the typical vorticity intensity. The latter number measures the importance of vortical overturning with respect to directional swimming.[13] Given the flow, specified in Sec. II B, the values of these two numbers determine the behavior of the swimming cells.

In Sec. IV, we will also consider the presence of stochastic terms (rotational Brownian motion) in Eq. (2).

B. The Kolmogorov flow

As discussed in the Introduction, gyrotactic cells in vertical shears can form thin layers when shear vorticity exceeds the inverse orientation time, i.e., when $\Psi > 1$, as demonstrated in laboratory experiments.[4] However, shear-induced turbulence can dissolve the layers after a finite lifetime. The process of TPL break-up due to turbulent fluctuations and thus the persistence properties of TPLs are still poorly characterized, mainly because of the experimental difficulties in tracking TPLs from birth to death.[25] Aiming to numerically explore the effects of turbulent fluctuations on the gyrotactic trapping, we consider here the periodic shear flow originally introduced by Kolmogorov to study the transition to turbulence. Several analytical studies have investigated its linear stability properties and weakly nonlinear behavior.[29] Moreover, extensive numerical simulations have explored the fully turbulent regime.[31,34]

The Kolmogorov flow is realized when the Navier-Stokes equation for an incompressible fluid ($\boldsymbol{\nabla}\cdot\boldsymbol{u} = 0$) is sustained via the Kolmogorov body force, i.e.,

$$\partial_t\boldsymbol{u} + \boldsymbol{u}\cdot\boldsymbol{\nabla}\boldsymbol{u} = -\boldsymbol{\nabla}p + \nu\Delta\boldsymbol{u} + F\cos(z/L)\hat{\boldsymbol{x}}, \tag{3}$$

where p is the pressure, density is taken to unity $\rho = 1$, and $\hat{\boldsymbol{x}}$ denotes the unit vector in the horizontal direction. The physical domain is a cube of size $L_B = 2\pi L$ with periodic boundary conditions in all directions. It is easy to verify that (3) admits a stationary solution, the *laminar* Kolmogorov flow $\boldsymbol{u} = U\cos(z/L)\hat{\boldsymbol{x}}$ with $U = L^2F/\nu$. This laminar solution becomes unstable with respect to transverse perturbations on scales larger than L when the Reynolds number, $Re = UL/\nu$, exceeds the critical value $Re_c = \sqrt{2}$. The first instability is two-dimensional (thanks to the Squire's theorem, valid for 2D, parallel flows) but, by increasing Re, three-dimensional motion develops and the flow eventually

becomes turbulent.[31,34] Remarkably, even in the fully developed turbulent state the mean velocity profile $\bar{\boldsymbol{u}}$ (the over-bar denoting time average) remains monochromatic, as in the laminar flow, i.e., $\bar{\boldsymbol{u}} = U\cos(z/L)\hat{\boldsymbol{x}}$, with a different amplitude $U < L^2F/\nu$.[34] By changing the relative amplitude of the turbulent fluctuations with respect to the mean Kolmogorov flow, we will investigate the effects of turbulence on shear-induced gyrotactic trapping, and thus on the persistence and properties of the resulting thin layers.

III. SWIMMING IN THE LAMINAR KOLMOGOROV FLOW

We start considering gyrotactic microorganisms swimming in a laminar Kolmogorov flow $\boldsymbol{u} = U\cos(z/L)\hat{\boldsymbol{x}}$. It is useful to make Eqs. (1) and (2) non-dimensional by measuring lengths, velocities, and times in terms of L, U, and L/U. In particular, Eq. (1) reads

$$\dot{X} = \cos Z + \Phi \mathrm{p}_x, \tag{4}$$

$$\dot{Y} = \Phi \mathrm{p}_y, \tag{5}$$

$$\dot{Z} = \Phi \mathrm{p}_z\,, \tag{6}$$

where $\Phi = v_s/U$ is the swimming number, while Eq. (2) becomes

$$\dot{\mathrm{p}}_x = -\frac{1}{2\Psi}\mathrm{p}_x\mathrm{p}_z - \frac{1}{2}\sin Z\,\mathrm{p}_z, \tag{7}$$

$$\dot{\mathrm{p}}_y = -\frac{1}{2\Psi}\mathrm{p}_y\mathrm{p}_z, \tag{8}$$

$$\dot{\mathrm{p}}_z = \frac{1}{2\Psi}(1-\mathrm{p}_z^2) + \frac{1}{2}\sin Z\,\mathrm{p}_x\,, \tag{9}$$

where $\Psi = BU/L$ is the stability number. The box size in dimensionless units is $L_B/L = 2\pi$.

The coordinates X and Y do not enter the dynamics of the other variables, thus we can ignore them and limit our analysis to the four dimensional dynamical system given by Eq. (6) for the vertical position and Eqs. (7)–(9) for the swimming orientation. The condition $|\mathbf{p}| = 1$ implies that the dynamics is three-dimensional.

It is easily seen from Eqs. (7) to (9) that when $\Psi \leq 1$ the gravitational bias dominates allowing cells to swim upwards through the vertical shear. Conversely, for $\Psi > 1$ vorticity becomes important inducing tumbling motion, which in turns gives rise to gyrotactic trapping.[4] In fact, seeking for an equilibrium swimming direction in Eqs. (7)–(9) when $\Psi > 1$, a refined analysis[1] shows that, thanks to the absence of vorticity along the direction of gravity (as for the Kolmogorov flow here considered), the only possible equilibrium solution is one with $\mathbf{p}$ lying on the plane perpendicular to gravity and is nonlinearly unstable. Therefore, if $\Psi > 1$ vortical motion overcomes gravitational bias and cells perform tumbling motion for some height Z where they remain trapped. While this is generic for steady shear flows with vorticity perpendicular to gravity, for the specific case of the Kolmogorov flow it is possible to characterize the dynamical behavior in great details. Indeed we can notice that, besides $|\mathbf{p}|$, Eqs. (4)–(9) admit two additional conserved quantities implying that the system is integrable.

We start our analysis by observing that, when the gravitational bias dominates the orientation dynamics (i.e., $\Psi < 1$), we expect an average upward swimming speed $\langle\dot{Z}\rangle = \Phi\langle \mathrm{p}_z\rangle > 0$. Since Eq. (8) is formally solved by $\mathrm{p}_y(t) = \mathrm{p}_y(0)\exp[-\int_0^t \mathrm{p}_z(s)ds/(2\Psi)]$, at long times we can write $\mathrm{p}_y(t) = \mathrm{p}_y(0)\exp[-t\langle \mathrm{p}_z\rangle/(2\Psi)]$, meaning that asymptotically $\mathrm{p}_y \to 0$ and the swimming orientation evolves on the $(\mathrm{p}_x, \mathrm{p}_z)$ plane. Actually, we can say more: dividing (8) by (6) yields $d\mathrm{p}_y/dZ = -\mathrm{p}_y/(2\Psi\Phi)$, which implies that

$$\mathcal{C}(\mathbf{p}, Z) = \mathrm{p}_y e^{Z/(2\Phi\Psi)} \tag{10}$$

is invariant under the dynamics (6)–(9). Furthermore, dividing (7) by (6) and solving the resulting ordinary differential equation for $p_x = p_x(Z)$, one easily finds that

$$\mathcal{H}(\mathbf{p}, Z) = \Phi e^{\frac{Z}{2\Phi\Psi}} \left[p_x - \frac{\Psi(2\Phi\Psi \cos Z - \sin Z)}{1 + 4\Phi^2\Psi^2} \right], \tag{11}$$

is also conserved by the dynamics. In Refs. 10 and 11, similar considerations were used for studying prolate cells, such as bacteria, swimming in a Poiseuille flow.

The conservation of $\mathcal{C}$ implies that if Z increases p_y has to compensate decreasing exponentially, as discussed above. As a consequence, we can neglect, at this stage, swimming in the y direction (i.e., we set $p_y = 0$) and limit our analysis to the two-dimensional system

$$\dot{\theta} = \frac{1}{2\Psi} \cos\theta + \frac{1}{2} \sin Z, \tag{12}$$

$$\dot{Z} = \Phi \sin\theta\,, \tag{13}$$

where we have introduced polar coordinates for the swimming orientation, $(p_x, p_z) = (\cos\theta, \sin\theta)$.

Since Eqs. (12) and (13) are periodic, we can consider the evolution on the torus $(\theta, z) \in [-\pi, \pi] \times [0 : 2\pi]$. In the following, we will use Z to denote the vertical coordinate and z to indicate its restriction to the torus (i.e., $z = Z \mod 2\pi$). We observe that the quantity (11) is not periodic in Z: when $Z \to Z \pm 2\pi n$, we have $\mathcal{H}(\theta, z) \to \mathcal{H}(\theta, z) e^{\pm \pi n/(\Phi\Psi)}$, i.e., $\mathcal{H}$ is multiplied by a constant.

The system (12)–(13) can be rewritten as

$$\begin{aligned} \dot{\theta} &= G(\theta, Z)\partial_Z \mathcal{H} \\ \dot{Z} &= -G(\theta, Z)\partial_\theta \mathcal{H} \end{aligned} \tag{14}$$

with $G = \exp[-Z/(2\Phi\Psi)]$ being the inverse integrating factor.[35,36] Therefore, the time change $t \to tG^{-1}$ makes (14) a Hamiltonian system having exactly the same trajectories of the original system (12)–(13) but these are traveled with different speeds. As a consequence, while the Lebesgue measure is invariant (from Liouville theorem) for the Hamiltonian system, this is not the case for Eqs. (12)–(13), which explains why one can observe accumulations of swimmers (see below).

Let us now inspect Eqs. (12)–(13) more closely. For $\Psi < 1$, the dynamics does not admit fixed points, and Z grows in time, as discussed above. The conservation of $\mathcal{H}$, and in particular the exponential dependence on Z, implies that when cells migrate upwards the term in square brackets in (11) must decrease exponentially with the vertical position to keep $\mathcal{H} = \text{const}$. Therefore, for large Z, the swimming direction will be given by

$$\cos\theta = p_x = \frac{\Psi(2\Phi\Psi \cos Z - \sin Z)}{1 + 4\Phi^2\Psi^2}\,. \tag{15}$$

Remarkably, because $p_z = \sqrt{1 - p_x^2}$ depends on Z, the vertical velocity will change with height and cells will accumulate where it is minimal. A straightforward computation shows that the minima of p_z occur at $Z = n\pi - \arctan[1/(2\Phi\Psi)]$, for any integer n. Around these positions one expects to observe ephemeral layers (also for $\Psi < 1$) of high density of cells. The transient accumulations last longer for smaller values of the swimming number Φ. The above picture is confirmed in Fig. 1(a) showing the time evolution of the vertical probability density distribution (PDF), $\rho(Z, t)$, resulting from an initially uniform distribution in $Z \in [0 : 2\pi]$ for $\Psi < 1$.

The above scenario applies whenever Eq. (15) holds globally, i.e., for any values of Z. As $|p_x| \leq 1$, it is easy to see that for swimmers with $\Phi < \Phi_c = 1/2$, Eq. (15) can be satisfied only if $\Psi \leq \Psi_c$ with

$$\Psi_c = (1 - 4\Phi^2)^{-1/2}\,. \tag{16}$$

For fast enough swimmers, $\Phi \geq \Phi_c$, Eq. (15) holds for any value of the stability number Ψ. As $\Psi_c \geq 1$, we must distinguish two cases.

In the first (Fig. 1(b)), $1 < \Psi < \Psi_c$, a fraction of cells migrate upwards asymptotically setting their motion on the orbit (15), as in Fig. 1(a) for cells with $\Psi < 1$. Also in this case maxima of cell density correspond to minima of p_z. However, unlike the case $\Psi < 1$, we now observe a

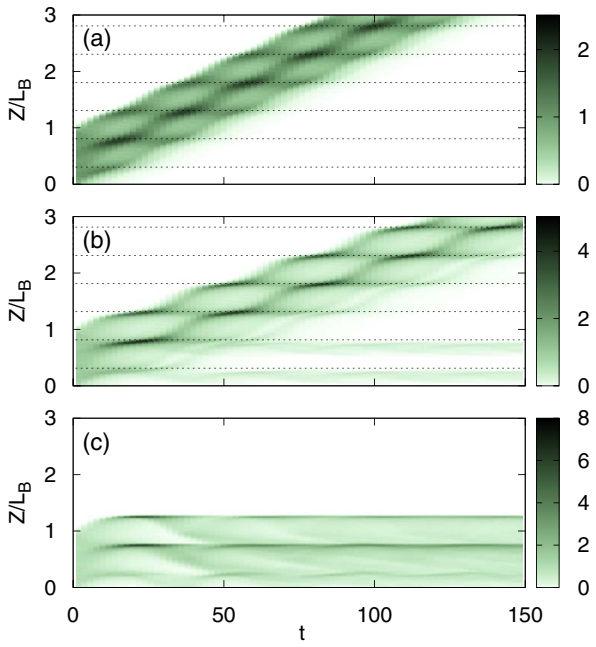

FIG. 1. Evolution of the vertical density of cells, $\rho(Z, t)$, in the 2d laminar Kolmogorov flow for $\Phi = 0.2$ with (a) $\Psi = 0.9 < \Psi_c$, (b) $1 < \Psi = 1.06 < \Psi_c$, and (c) $\Psi = 1.12 > \Psi_c$, where Ψ_c is given by (16). Dotted horizontal lines in (a) and (b) mark vertical velocity minima (see text for a discussion). The density has been obtained by coarse-graining the vertical position of $N = 10^4$ cells initialized uniformly in $(\theta, Z) \in [-\pi, \pi] \times [0 : 2\pi]$ and evolved by integrating Eqs. (12) and (13) with a 4th-order Runge-Kutta scheme.

non-negligible fraction of cells (depending on the initial conditions) which do not migrate upwards and accumulate in thin layers, now not in correspondence of the minima of p_z (Fig. 1(b)).

In the second, $\Psi > \Psi_c$, we observe that all swimmers become trapped and generate an inhomogeneous vertical density profile which soon becomes stationary in time and organized in thin layers (Fig. 1(c)).

We can understand the different behaviors observed in Figs. 1(b) and 1(c) by inspecting the phase-space qualitative dynamics for $1 < \Psi < \Psi_c$ and $\Psi > \Psi_c$. First, we observe that, for $\Psi > 1$, Eqs. (12) and (13) admit the following fixed points (written in the reference torus)

$$(\theta^*, z^*) = \begin{cases} H1\ (0, 2\pi - \arcsin(\Psi^{-1})) \\ H2\ (\pi, \pi - \arcsin(\Psi^{-1})) \\ E1\ (0, \pi + \arcsin(\Psi^{-1})) \\ E2\ (\pi, \arcsin(\Psi^{-1}))\,, \end{cases} \tag{17}$$

where H's and E's are hyperbolic and elliptic fixed points (see Fig. 2) with eigenvalues $\lambda = \pm(\Phi\sqrt{1-\Psi^{-1}}/2)^{1/2}$ and $\pm i(\Phi\sqrt{1-\Psi^{-1}}/2)^{1/2}$, respectively.

Below and above the critical value Ψ_c the form of the separatrices, i.e., the orbits emerging from the hyperbolic fixed points, changes qualitatively. For $1 < \Psi < \Psi_c$ the separatrices roll up vertically around the torus with a slip-knot from the hyperbolic point containing the elliptic one (see Fig. 2(a)). Orbits initially within the slip-knot remain trapped there, while those starting outside the slip-knot migrate vertically, asymptotically following the orbit (15). Conversely, when $\Psi > \Psi_c$, the separatrices roll up around the torus in the θ direction (Fig. 2(b)) acting as barriers to vertical transport as typically happens in Hamiltonian systems.[37] Hence, whenever $\Psi > \Psi_c$ trajectories remain bounded in the vertical direction for all initial conditions. It is noted that for $\Psi = \Psi_c$, the orbit (15) becomes the separatrix and passes through all the hyperbolic points. Figure 3 summarizes the possible behaviors in parameter space (Φ, Ψ).

It should be noted that this layered structure is essentially due to the fact that: (i) the velocity on the orbit depends on the vertical position, and the trajectory spends more time where G is smaller

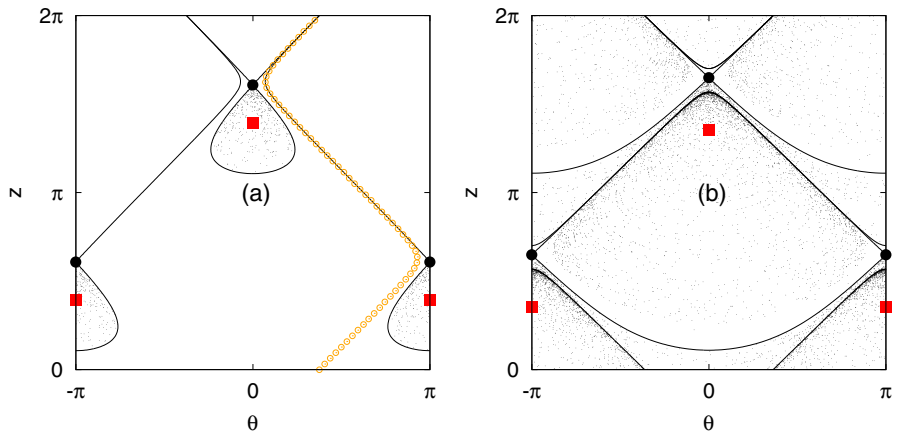

FIG. 2. Cells positions in the laminar 2D Kolmogorov flow at a long time on the (θ, z) torus for (a) $\Psi = 1.06$ and (b) $\Psi = 1.12$ with $\Phi = 0.2$, corresponding to Figs. 1(b) and 1(c), respectively. Black circles (red squares) mark the hyperbolic (elliptic) fixed points (17). Black curves denote the separatrices emerging from the hyperbolic fixed points, which are obtained from the isolines of $\mathcal{H}$ computed at $H1$ and $H2$. At $\Psi < \Psi_c$ (a) small black dots corresponds to trapped orbits and empty circles to the orbit (15) which asymptotically characterizes the vertically migrating cells and is very close to the separatrix. For $\Psi > \Psi_c$ (b) all orbits are trapped.

(i.e., Z large) as from Eq. (14); (ii) the fact that the separatrices confine the motion. It is easy to understand that (i) and (ii) imply that concentration will be large around the highest allowed vertical value which, for $1 < \Psi < \Psi_c$ (Fig. 2(a)), coincides with the hyperbolic points and, for $\Psi > \Psi_c$ (Fig. 2(b)), is in between the hyperbolic and elliptic points. Cell accumulation will thus increase going upwards to the top of the separatrices and then will abruptly fall down, as revealed by the vertical asymmetry in density profiles shown in Fig. 4, see also Ref. 25 for a discussion on such asymmetries.

It should be noted that at increasing Ψ, the accumulation in layers tends to disappear (see also Fig. 4). Indeed in the limit $\Psi \to \infty$, the dynamics (12)–(13) becomes Hamiltonian with $\mathcal{H} = \Phi \cos\theta - (1/2)\cos(Z)$, corresponding to the well-known Harper Hamiltonian, originally introduced to describe crystal electrons in the presence of a magnetic field.[38] Consequently, swimming cells

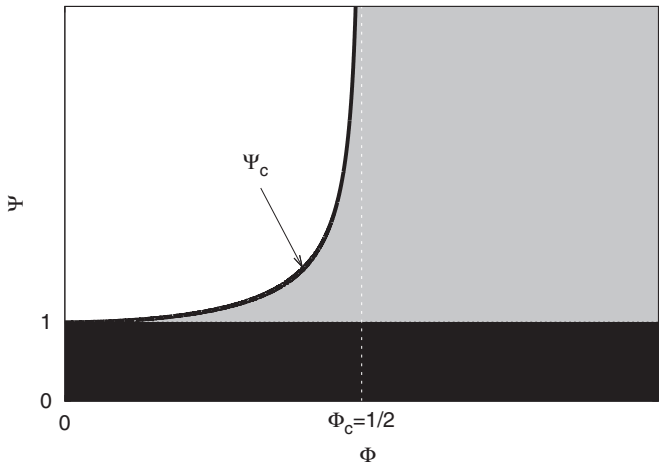

FIG. 3. Behavior of swimming cell in parameter space for the laminar Kolmogorov flow. The white region corresponds to vertically trapped orbits ($\Psi > \Psi_c$), the grey one to partially trapped trajectories ($1 < \Psi < \Psi_c$), with coexistence of trapped and vertically migrating cells) and, finally, the black to vertically migrating cells ($\Psi < 1$), whose swimming direction depends on the vertical position as predicted by Eq. (15).

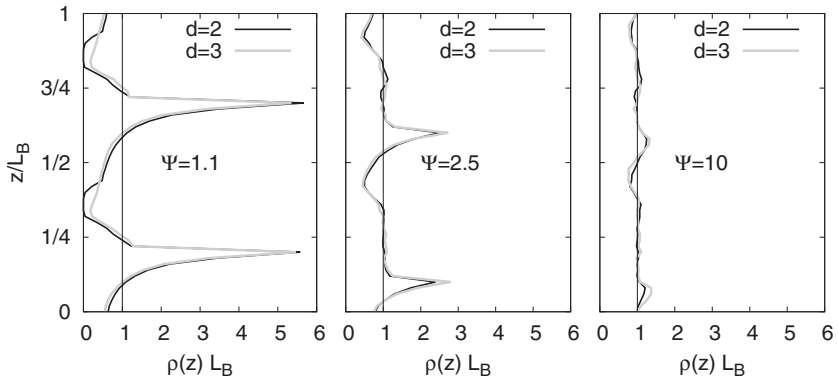

FIG. 4. Number density of algae corresponding to the two layers in the periodic domain $z \in [0 : L_B]$, for both 2D and 3D for $\Phi = 0.05$ and three values of Ψ as labeled. Density differs for minor details in the two cases. Notice that layers tend to disappear for large Ψ.

cannot display accumulation as implied by Liouville theorem. Nonetheless, provided $\Phi < \Phi_c$, also in this limit we have that the separatrices act as barriers to vertical migration.

We conclude this section briefly commenting the three-dimensional case. As discussed above, thanks to the invariance of (10) upward migrating cells (as in the black and grey region of Fig. 3) follow trajectories which a long times coincide with the two-dimensional case (as $p_y \to 0$). In principle, the dynamics of non-vertically-migrating cells can be fully characterized, e.g., studying the conserved quantities.[10] On a qualitative level, the orientation vector will move on the intersection between the surface determined by (10) and (11) and the sphere $|\mathbf{p}| = 1$. The conservation of (10) implies that the extreme values reached by p_y are linked to the extremes of Z. The same conservation law also shows that p_y is bounded away from 0 for any finite Z and any initial condition with $p_y \neq 0$. As a consequence, all bounded trajectories will have a finite average drift along y, according to the initial sign of p_y. However, since y is a slaved variable, the above depicted scenario, including the behavior in parameter space (Fig. 3) is unmodified going from two to three dimensions. Actually, as shown in Fig. 4, the (vertical) density profiles are quantitatively very close in two and three dimensions.

IV. EFFECTS OF ROTATIONAL DIFFUSION

In this section, we focus on the effects of stochasticity on the dynamics of the swimming orientation. Even in a still fluid, indeed, swimming trajectories are not straight lines and usually display a certain degree of randomness because of thermal fluctuations and/or of the swimming process. Thermal fluctuations are important for very small ($\sim 1\mu$m) microorganisms, e.g., bacteria, and can be modeled in terms of rotational Brownian motion (RBM),[15] namely, as a diffusion of the swimming direction on the unit sphere. Gyrotactic microalgae are typically too large to be affected by thermal fluctuations. However, in theoretical approaches[2,39] and consistently with experimental observations,[40,41] it is still possible to use RBM to model the random fluctuations of the swimming direction due, e.g., to small variations in the cell shape, waving or imperfections in the flagella movement, and bacteria-like run-and-tumble[42] due to the desynchronization between the flagella.

For the sake of simplicity, we only consider the 2D Kolmogorov flow, which displays, also quantitatively (see, e.g., Fig. 4), the main features of the 3D flow. In two dimensions, RBM corresponds to diffusion of the angle θ in Eq. (12) with (rotational) diffusivity D_r. As an example, in *Chlamydomonas augustae*[6] $D_r^{-1} \sim 15\,s$. It is useful to introduce a non-dimensional measure of diffusion, namely, the rotational Peclet number $Pe_r = U/(LD_r)$. Considering RBM amounts to adding to the r.h.s. of (12) the stochastic term $\sqrt{2Pe_r^{-1}}\eta$, η being a zero-mean Gaussian variable with $\langle \eta(0)\eta(t)\rangle = \delta(t)$.

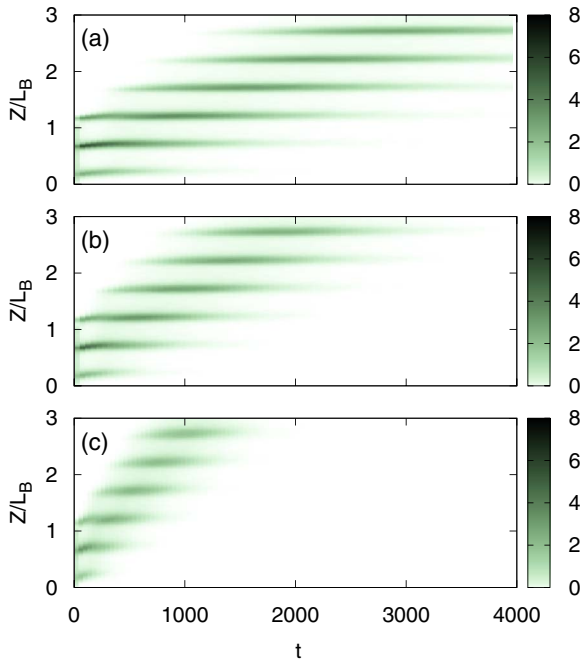

FIG. 5. Evolution of the vertical number density $\rho(Z, t)$ in the 2D laminar Kolmogorov flow with parameter as in Fig. 1(c) and the presence of rotational Brownian motion with (a) $Pe_r^{-1} = 0.005$, (b) 0.01, and (c) 0.04.

RBM can cause dramatic effects when gyrotactic trapping is effective (i.e., when $\Psi > \Psi_c$): in principle, for any $Pe_r^{-1} > 0$, thanks to random fluctuations, all swimmers potentially have a way to escape from the "barrier" of the separatrices (by definition, impenetrable in the deterministic case). We therefore expect that a small random component in the swimming dynamics will make layers transient, with a finite lifetime.

This scenario is confirmed in Fig. 5 showing the time evolution of the vertical cell-number density for stability number corresponding to gyrotactic trapping (with $\Psi > \Psi_c$ as in Fig. 1(c)) when RBM is acting on the dynamics. Similar to the deterministic case, an initially uniform distribution in $(\theta, Z) \in [-\pi : \pi] \times [0 : L_B]$ (quickly) evolves into layers located around the elliptic points. However, unlike the deterministic case, after a typical time depending on Pe_r, any layer dissolves and, thanks to the flow periodicity, gives birth to a new layer at distance $L_B/2$ upward. The "length" of the traces in Fig. 5 essentially corresponds to the lifetime of a layer. Clearly, in the case of a non-periodic set-up only a single layer would form, persist for some time and then dissolve unless a continuous in-flow of algae is provided from below. We notice that the lowest layer lasts for about half the duration of the other layers: this is due to the fact that it has no layers below feeding it. The figure shows that the value of Pe_r influences both the lifetime and the focusing of the layers. We shall be more quantitative on this aspect in the following.

To better understand the process it is useful to inspect the behavior of a typical single swimmer trajectory (Fig. 6). We can clearly identify trapped states interrupted by rapid upward migrations. As from Fig. 2(b), trapping is spatially localized at Z values (mainly) in between adjacent elliptic and hyperbolic points, where a swimmer can spend a long time before RBM allows it to escape the separatrix. Out of the trapping region, shear vorticity is low and thus the cell can locally migrate vertically (as globally done when $\Psi < 1$), till it enters a new trapping region shifted of $L_B/2$ above due to the flow periodicity. Then the process starts again. The (stochastic) switch between these two states of motion induces an average vertical drift, $\langle v_z \rangle > 0$ (Fig. 7(a)). Clearly, in both the deterministic ($Pe_r^{-1} \to 0$) and RBM dominated (large Pe_r^{-1}) we should expect a zero average drift: in the former case because of gyrotactic trapping, in the latter due to fast decorrelation of the swimming orientation due to RBM (this is expected when $\Psi/Pe_r = BD_r$ becomes very large). Consequently, we expect to

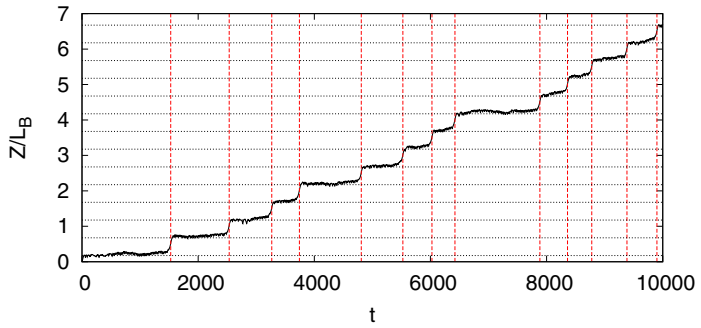

FIG. 6. Typical cell trajectory for $\Phi = 0.05$, $\Psi = 1.12$, and $Pe_r^{-1} = 0.005$. We can identify two regimes: temporary trapping in a layer (around the horizontal dashed lines demarking the elliptic points) and short jumps between layers. Vertical (red) lines mark the transition between adjacent layers, numerically identified as the times at which the vertical position Z increases of $L_B/2$.

have an intermediate value of the rotational diffusivity for which the vertical drift is maximal, as confirmed in Fig. 7(a).

The qualitative features of the trajectory shown in Fig. 6 suggest to look at the statistics of trapping time T. Thanks to the periodicity and the fact that out of the layer vertical migration is fast (Fig. 6), we can define it as the time T it takes for a swimmer to swim upwards the distance between two consecutive layers (i.e., $L_B/2$ in our model flow). The average exit (or trapping) time $T_e = \langle T \rangle$ shown in Fig. 7(b) coincides with $L_B/(2\langle v_z \rangle)$. While this is obvious as the two statistics are mathematically equivalent, it can be useful when coping with finite observation times. In fact, exit-time statistics can be strongly biased when the total observation time is not large enough (see Sec. V).

A quantitative comparison between the average exit time T_e of the single trajectory and Fig. 5 suggests however that T_e tends to underestimate the layers time duration. A more sound definition of the layer persistence time, T_p, requires somehow to account for the fact that there could be many swimmers trapped for times longer than the average T_e. Heuristically, we found that a reasonable estimate is obtained considering that a layer dissolves when, say, $\sim$90% of the cells have escaped from it. In terms of the exit time probability density function $p(T)$, we can thus define T_p implicitly as $\int_0^{T_p} p(T)dT \approx 0.9$. Fig. 7(b) shows also T_p, which appears to be a better proxy of the persistence time, for instance, in the case of Fig. 5(b), i.e., $Pe_r^{-1} = 0.01$, we have $T_p \approx 630$ which is essentially the trace length of the lowest layer, i.e., half of the other layers.

The interpretation of T_p as the layer persistence time, however, becomes meaningless when layers are not well defined. For example, from Fig. 7(b) one can get the wrong impression that at large D_r layers last longer and longer. In reality, by increasing D_r (i.e., decreasing the coherence in the swimming orientation) layers spread away, becoming less and less well defined as high cell density locations (as when Ψ becomes too large, see Fig. 4). To quantify such an effect, we introduce a measure based on the quadratic deviation from the uniform distribution on the domain $z \in [0 : L_B]$. In other terms we use the periodicity to restrict the vertical position in $z \in [0 : L_B]$ so that we can define the density $\rho(z, t)$. With RBM such density reaches a statistically stationary profile and we define the normalized root mean square deviation of the average profile, $\rho(z)$, from that expected for a uniform distribution, i.e., $\rho(z) = \rho_0 = 1/L_B$. In formulae, this *inhomogeneity index* is defined as

$$\chi = \sqrt{\langle (\rho - \rho_0)^2 \rangle}/\rho_0 \,, \tag{18}$$

the angular brackets denoting integration over z. Figure 7(c) shows that this measure monotonically decreases with D_r, as expected. Also, faster swimmers concentrate less.

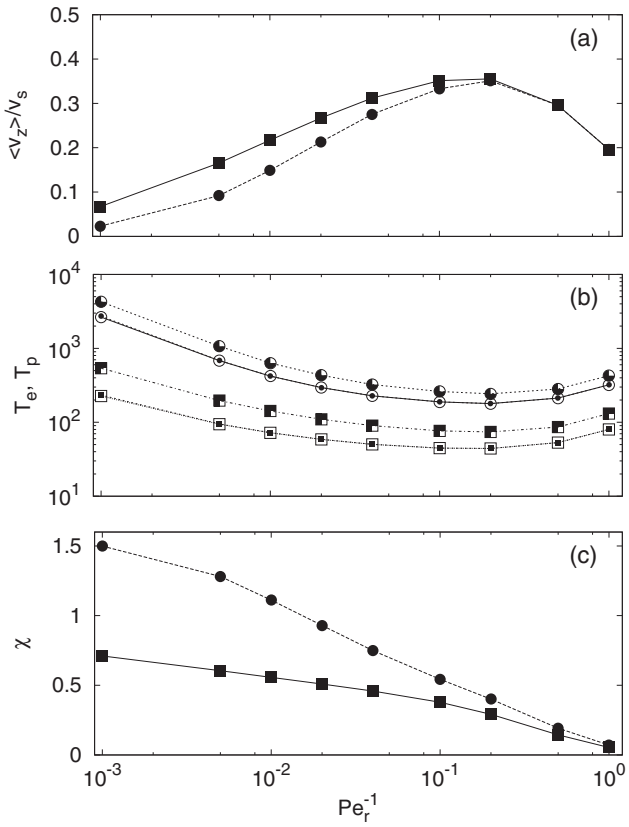

FIG. 7. Quantitative characterization of single cell and layer properties as a function of the rotational Peclet number Pe_r, for two values of the swimming parameter $\Phi = 0.05$ (circles) and $\Phi = 0.2$ (squares) at $\Psi = 1.12 > \Psi_c$ in the 2D laminar Kolmogorov flow. (a) Time and population average vertical velocity $\langle v_z \rangle$ normalized to the swimming speed v_s. (b) Average trapping time T_e (open symbols) for single trajectories and layer persistence time T_p (semi-filled symbols). Notice that the exit time T_e coincides with $L_B/(2\langle v_z \rangle)$ (small filled symbols inside the empty ones). (c) Inhomogeneity index χ defined in (18).

V. SWIMMING IN THE TURBULENT KOLMOGOROV FLOW

As discussed in Sec. II B, the steady Kolmogorov flow becomes unstable for $\mathrm{Re} > \sqrt{2}$ and ultimately turbulent, upon further increasing Re. Nonetheless, thanks to the monochromatic character of the (time-averaged) mean flow, we can always decompose velocity and vorticity, entering Eqs. (1) and (2), in the mean shear with superimposed fluctuations $\boldsymbol{u}'$ and $\boldsymbol{\omega}'$ as

$$\boldsymbol{u} = U \cos(z/L)\hat{\boldsymbol{x}} + \boldsymbol{u}'(\boldsymbol{x}, t), \tag{19}$$

$$\boldsymbol{\omega} = -\frac{U}{L} \sin(z/L)\hat{\boldsymbol{y}} + \boldsymbol{\omega}'(\boldsymbol{x}, t)\,. \tag{20}$$

Such decomposition suggests that we can consider turbulent fluctuations as a perturbation of the dynamics studied in Sec. III. Actually, even at relatively low *Re*, the amplitude of turbulent fluctuations is of the same order as the mean flow, in particular $u'_{\mathrm{rms}}/U \simeq 0.5$.[34] In real oceans, however, fluctuations are typically smaller than the mean flow due to different factors, e.g., stratification.[33]

In the following, we will therefore consider the velocity (and vorticity) field defined as $U\cos(z/L)\hat{\boldsymbol{x}} + \gamma \boldsymbol{u}'$, where $\boldsymbol{u}'$ is the fluctuating component in (19), obtained by a direct numerical simulation (DNS) of Eq. (3). In this way, the parameter γ controls the intensity of turbulent fluctuations so that $u'_{\mathrm{rms}}/U \simeq 0.5\gamma$. The ability to control the weight of fluctuations is important to systematically assess the role of fluctuations. Indeed, as we shall see below, in the standard Kolmogorov flow (i.e., $\gamma = 1$), turbulence is so intense to completely dissolve phytoplankton layers.

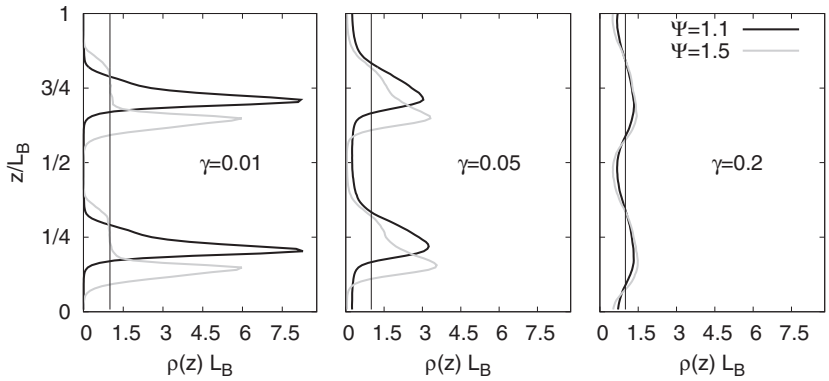

FIG. 8. Vertical profile of swimmer number density $\rho(z)$ for two values of the stability parameter $\Psi = 1.1$ (black lines) and $\Psi = 1.5$ (grey lines) at different turbulent intensities $\gamma = 0.01$, $\gamma = 0.05$, and $\gamma = 0.2$ (from left to right).

Another advantage of this approach is that the statistical properties of the turbulent fluctuations do not change with γ as they would, for example, by introducing stratification.

Navier-Stokes equations (3) are integrated by means of a standard, fully parallel pseudo-spectral code[34] on a cubic domain of size L_B discretized by 128^3 grid points, with periodic boundary conditions in all directions. Lagrangian dynamics (1)–(2) (suitable modified with the γ-factor as discussed above) of up to 10^5 swimmers for each set of parameters (Φ, Ψ, γ) was performed using linear interpolation of the velocity and vorticity fields, as in Refs. 13 and 14. A 2nd-order Runge-Kutta scheme was used for time advancement of both Eulerian and Lagrangian dynamics. Particle positions were re-boxed within the periodic domain in the x and y directions, while the absolute displacement was tracked along z. The Reynolds number in our simulation is $Re = 158$, the smallest Kolmogorov scale η is well resolved as $k_{\max}\eta \approx 1.8$.

Turbulent fluctuations, when strong enough, inhibit gyrotactic trapping. This is confirmed in Fig. 8, showing the swimmer vertical-density profiles for $\Psi = 1.1$ and $\Psi = 1.5$ at varying the intensity of turbulent fluctuations γ. Upon increasing γ vertical heterogeneity weakens. This effect is quantified by the inhomogeneity index χ Eq. (18), shown in Fig. 9 as a function of the stability parameter Ψ for three values of the turbulent intensity γ. As in Sec. IV, we focus here on the case $\Psi > \Psi_c$, when gyrotactic trapping is effective in the laminar regime. Interestingly, at increasing γ turbulent fluctuations not only smooth the inhomogeneities (decreasing the value of χ) but also induce a non-monotonic dependence on Ψ, with maximal inhomogeneity obtained for a value of the stability parameter, $\Psi \gtrsim \Psi_c$, weakly depending on γ.

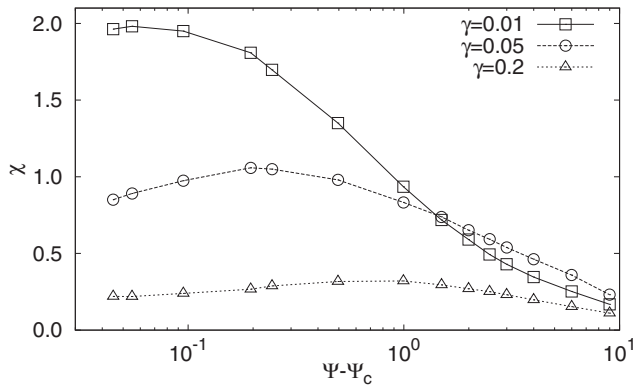

FIG. 9. Inhomogeneity index χ as a function of Ψ for various γ. Data symbols are shown only for values of the stability number such that gyrotactic trapping is effective in the laminar case, i.e., $\Psi > \Psi_c$.

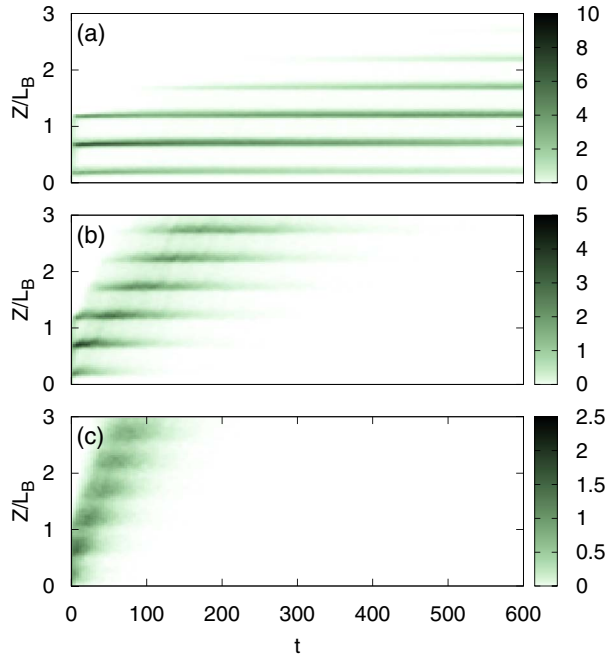

FIG. 10. Evolution of vertical density of cells in a turbulent Kolmogorov flow for swimming parameters $\Psi = 1.1$, $\Phi = 0.05$ and turbulence intensity $\gamma = 0.01$ (a), 0.05 (b), 0.2 (c). The initial condition is a random uniform distribution on $[0, L_B]$. Subsequent formation and disruption of layers is evident in panels (b) and (c) (compare with the laminar case in presence of rotational diffusion shown in Fig. 5). Time and scale have been made non-dimensional as for the laminar case.

Figure 10 shows the formation and disruption of layers, similar to the phenomenology induced by RBM (Fig. 5). More quantitatively, Figure 11 shows the average vertical velocity $\langle v_z \rangle$, escape and persistence times $T_{e,p}$ and inhomogeneity index as a function of γ, which plays a similar role of Pe_r^{-1} for the laminar case with RBM (compare with Fig. 7).

At moderate values of turbulent intensity, velocity and vorticity fluctuations allow cells to escape from the trapping regions by moving them to regions of lower shear, where upward directed swimming is possible. As a result, the average vertical cell velocity, $\langle v_z \rangle$, which was zero in the absence of turbulent fluctuations, becomes positive. However, very intense turbulence rotates the cell swimming direction randomly and, moreover, fluctuations of the vertical velocity also mix cells. As a consequence, the average vertical motion $\langle v_z \rangle$ decreases for large values of γ. An intermediate turbulence intensity maximizes the vertical migration velocity (see Fig. 11(a)). The average exit time, as already discussed, is determined by the average swimming speed, i.e., $T_e = L_B/(2\langle v_z \rangle)$ (Fig. 11(b)). However, unlike the laminar case (Fig. 7(b)), here the agreement is not perfect especially when T_e is large. The reason is that the total integration time of turbulent simulations was shorter and the exit-time statistics does not converge for very large T. In realistic situations, where the numerical or experimental time is finite, the evaluation of T_e must be carefully performed and compared with the other statistics such as the average vertical velocity. The most affected cases are the ones with very weak or very intense turbulence. In the latter case, $\chi \approx 0$ and thus layering is negligible.

A simple way to model the vertical dynamics of gyrotactic swimmers is in terms of a diffusive process with drift V_d (due to the average vertical migration speed, i.e., $V_d = \langle v_z \rangle$) and diffusion constant D_z, whose value depends on turbulent fluctuations. The escape from a layer can then be addressed through the exit-time statistics asking for the time T needed for a swimmer to travel a distance $L_B/2$. This is a standard problem in stochastic processes, see, e.g., Ref. 43. In the case of diffusion with drift, the probability density function of the exit time T is given by the so-called inverse Gaussian function, which we can write as follows:

$$\mathcal{P}(T) = \frac{L_B}{(4\pi D_z T^3)^{1/2}} e^{-\frac{(V_d T - L_B/2)^2}{4 D_z T}} . \tag{21}$$

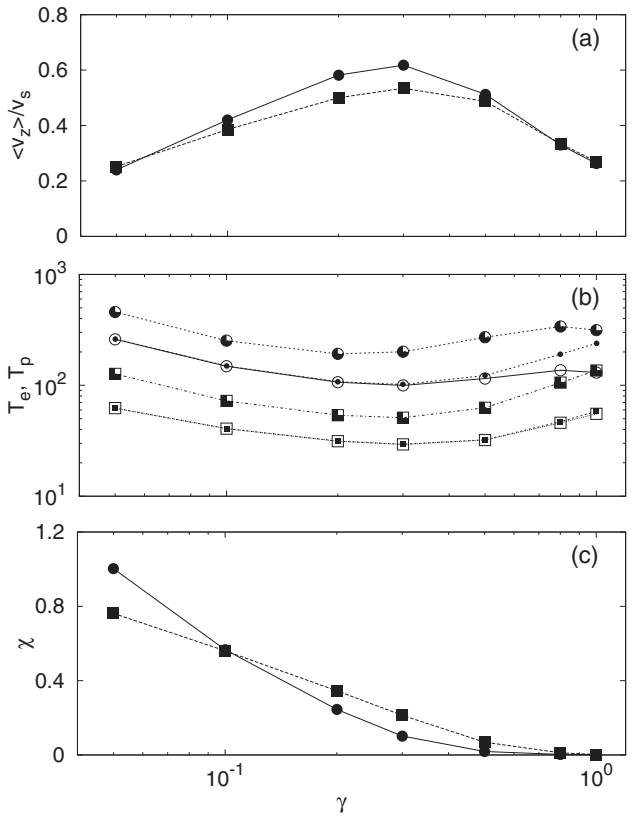

FIG. 11. Quantitative characterization of single cell and layer properties as a function of turbulent intensity γ, for $\Phi = 0.05$ (circles) and $\Phi = 0.2$ (squares) with $\Psi = 1.1$. (a) Average vertical velocity $\langle v_z \rangle$ normalized to the swimming speed v_s. (b) Layer persistence time T_p (semi-filled symbols) and average trapping time T_e (open symbols) for single trajectories, compared to $L_B/(2\langle v_z \rangle)$ (small filled symbols inside the empty ones). Notice the discrepancy between $\pi/\langle v_z \rangle$ and T_e at $\Phi = 0.2$, see text for a discussion. (c) Inhomogeneity index χ as from Eq. (18).

We thus have a prediction for the exit time PDF which can be directly tested against the measured one. For the drift velocity we have $V_d = \langle v_z \rangle$, which is measured in DNS (Fig. 11(a)), notice also that Eq. (21) implies $T_e = \langle T \rangle = L_B/(2V_d)$, consistently with Fig. 11(b). The diffusion constant D_z can be estimated by measuring $\langle T^2 \rangle$ in the DNS and noticing that in Eq. (21) $\langle T^2 \rangle = L_B(D_z + LV_d/2)/V_d^3$. In Figure 12(a), we show the comparison between measured exit-time PDF $p(T)$ and the inverse Gaussian prediction (21), with D_z and V_d obtained as discussed above. The prediction turns out to be very accurate for the right tail (long exit times) for all turbulent intensities γ, while the left tail reproduces the numerical results only for large values of γ. Indeed a purely Gaussian model cannot be expected to describe the escape-time statistics accurately in presence of strong trapping. The deviations in the left tails can be interpreted as the result of the suppression of fast escapes due to gyrotactic trapping, which is more effective in the limit $\gamma \to 0$. On the other hand, long escape times allow trajectories to sum-up many uncorrelated contributions, thus recovering a diffusive behavior, which explains the good agreement on the right tail.

It is natural to identify D_z with the vertical turbulent eddy diffusivity D_z^{turb}, characterizing the large scale diffusive properties of fluid tracers. In Figure 12(b) we show, as a function of the turbulent intensity γ, the D_z estimated from the exit-time statistics for different values of Φ and Ψ and the (vertical) turbulent diffusivity measured from the vertical mean square displacement of tracer particles in the same flow. We start by noticing that the turbulent diffusivity behaves as $D_z^{turb} \propto \gamma^2$, which is consistent with the expectations as $D_z^{turb} \propto (u'_{\rm rms})^2 \approx \gamma^2 (U/2)^2$. Then we observe that the diffusivity D_z for gyrotactic swimmers, estimated from exit times, is typically larger than the turbulent one, and the deviation is more pronounced at small γ for larger swimming number and

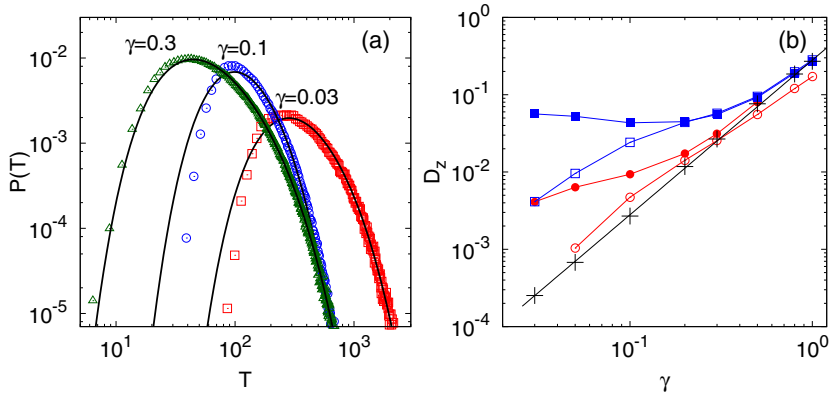

FIG. 12. Exit time statistics. (a) Exit time PDF for $\Psi = 1.1$, and $\Phi = 0.05$ at three turbulent intensities γ as labeled, compared with the prediction (21) with D_z and V_d obtained as explained in the text. (b) Vertical diffusivity constant D_z estimated from exit time statistics for cells with $\Phi = 0.05$ (red circles) and $\Phi = 0.2$ (blue squares) for $\Psi = 1.1$ (filled symbols) and $\Psi = 1.5$ (empty symbols). Statistical convergence is poor at large and small γ's for $\Phi = 0.05$. The solid black line displays the γ^2 behavior of the turbulent diffusivity measured along tracer trajectories (plus symbols).

smaller stability number, more precisely for Ψ closer to Ψ_c. These features can be rationalized as follows. In the presence of turbulent fluctuations, the vertical diffusivity is expected to have two contributions: one from the fluctuations of the vertical velocity, which can be estimated from turbulent diffusivity, and one from swimming combined with the reorientation of the swimming direction due to vorticity fluctuations. Clearly, the latter contribution will lead to a diffusivity which increases with the swimming speed and thus is more important than the former for small γ, indeed $v_s/u'_{\rm rms} \sim \Phi/\gamma$. This explains the larger discrepancy at small γ. As for the effect of stability, diffusivity due to swimming is expected to be larger when vertical motion is more coherent, i.e., cells are more stable in their orientation (i.e., Ψ is smaller). Finally, when turbulent fluctuations become the dominant effect, layers tend to disappear and cells are expected to recover a diffusive dynamics which explains the convergence of D_z to the turbulent value for $\gamma \to 1$. Consistently, the PDF of exit-times converges to (21) (see Fig. 12).

VI. CONCLUSIONS

In this paper, we have investigated the phenomenon of gyrotactic trapping which has been recently proposed as one of the possible mechanisms responsible for thin phytoplankton layer formation.[4,25]

We derived a detailed theory of the mechanism within the framework of dynamical systems theory for the laminar Kolmogorov flow. The ideas and tools here developed can be generalized to basically any laminar shear flow. In particular, the approach developed in Sec. III can be easily extended to Poiseuille-like velocity fields such as that used in the experiments presented in Ref. 4. Nonetheless the Kolmogorov flow is advantageous as it allows us to avoid considering boundaries and focus on bulk properties without the need to model the behavior of swimmers close to walls. Moreover, thanks to the fact that the sinusoidal mean profile is preserved in the turbulent case, we studied how gyrotactic trapping is altered by turbulence.

We found that turbulent fluctuations, similar to random fluctuations of swimming direction due to rotational Brownian motion, make gyrotactic trapping transient. We characterized the phenomenon in terms of trapping (or exit) times and showed that in the presence of turbulence the statistics of exit times can be modeled (at least for long trapping events) by a diffusive process with drift. In particular, the (vertical) drift velocity results from the average upward swimming, while diffusion results from both turbulent diffusivity (as for tracer particles) and swimming combined to fluctuations of the swimming direction. When velocity fluctuations are small compared to the swimming speed, the diffusivity induced by the latter is important. As a consequence, care should be taken when

estimating the effect of turbulence on thin layers formed by swimming phytoplankton in terms of turbulent diffusivity alone. Swimming combined to reorientation of the swimming direction can indeed be very important for the diffusivity properties, as also recently recognized in simple linear flows.[44]

We found that the average exit time of single trajectories T_e is given by the average swimming speed and typical vertical length characterizing the layers (which in the periodic Kolmogorov flow is $L_B/2$). The persistence time of the layer T_p is of the order of a few (typically $\sim 2-3$) T_e depending on the value of the vertical diffusivity, using, e.g., the inverse Gaussian prediction (21). Thus ignoring the aforementioned difficulties in estimating D_z for realistic oceanic flows, if we consider average swimming speeds $\langle v_z \rangle$ in the range $0.2-0.6\, v_s$, as suggested by Fig. 11(b) (with $v_s \approx 100-200\mu$m/s) and typical lengths L_B of the order of a few centimeters, we obtain an estimation of T_p from a few hours to a few days, which is akin to values found in TPLs observed on the field.

We conclude mentioning that it would be very interesting in future investigations to consider a more realistic model in which modulation of turbulent fluctuations are controlled by stratification, as in real oceans. Moreover, it would be useful to quantitatively assess the diffusion properties of swimming microorganism under the combined effect of swimming and fluid motion.

ACKNOWLEDGMENTS

We acknowledge useful discussions with Luca Brandt, Roman Stocker, and Roberto Tateo.

[1] T. J. Pedley and J. O. Kessler, "The orientation of spheroidal microorganisms swimming in a flow field," Proc. Royal Soc. B **231**, 47 (1987).
[2] T. J. Pedley and J. O. Kessler, "Hydrodynamic phenomena in suspensions of swimming microorganisms," Annu. Rev. Fluid Mech. **24**, 313 (1992).
[3] J. O. Kessler, "Hydrodynamic focusing of motile algal cells," Nature (London) **313**, 218 (1985).
[4] W. M. Durham, J. O. Kessler, and R. Stocker, "Disruption of vertical motility by shear triggers formation of thin phytoplankton layers," Science **323**, 1067 (2009).
[5] T. J. Pedley, N. A. Hill, and J. O. Kessler, "The growth of bioconvection patterns in a uniform suspension of gyrotactic micro-organisms," J. Fluid Mech. **195**, 223 (1988).
[6] C. R. Williams and M. A. Bees, "Photo-gyrotactic bioconvection," J. Fluid Mech. **678**, 41 (2011).
[7] J. Dunkel, S. Heidenreich, K. Drescher, H. H. Wensink, M. Bär, and R. E. Goldstein, "Fluid dynamics of bacterial turbulence," Phys. Rev. Lett. **110**, 228102 (2013).
[8] C. Torney and Z. Neufeld, "Transport and aggregation of self-propelled particles in fluid flows," Phys. Rev. Lett. **99**, 078101 (2007).
[9] G. J. Thorn and R. N. Bearon, "Transport of spherical gyrotactic organisms in general three-dimensional flow fields," Phys. Fluids **22**, 041902 (2010).
[10] A. Zöttl and H. Stark, "Nonlinear dynamics of a microswimmer in poiseuille flow," Phys. Rev. Lett. **108**, 218104 (2012).
[11] A. Zöttl and H. Stark, "Periodic and quasiperiodic motion of an elongated microswimmer in poiseuille flow," Europ. Phys. J. E **36**, 4 (2013).
[12] R. Chacón, "Chaotic dynamics of a microswimmer in poiseuille flow," Phys. Rev. E **88**, 052905 (2013).
[13] W. M. Durham, E. Climent, M. Barry, F. De Lillo, G. Boffetta, M. Cencini, and R. Stocker, "Turbulence drives microscale patches of motile phytoplankton," Nat. Commun. **4**, 2148 (2013).
[14] F. De Lillo, M. Cencini, W. M. Durham, M. Barry, R. Stocker, E. Climent, and G. Boffetta, "Turbulent fluid acceleration generates clusters of gyrotactic microorganisms," Phys. Rev. Lett. **112**, 044502 (2014).
[15] H. C. Berg, *E. coli in Motion* (Springer, Verlag, 2004).
[16] X. Garcia, S. Rafaï, and P. Peyla, "Light control of the flow of phototactic microswimmer suspensions," Phys. Rev. Lett. **110**, 138106 (2013).
[17] F. F. de Araujo, M. A. Pires, R. B. Frankel, and C. E. M. Bicudo, "Magnetite and magnetotaxis in algae," Biophys. J. **50**, 375 (1986).
[18] E. Malkiel, O. Alquaddoomi, and J. Katz, "Measurements of plankton distribution in the ocean using submersible holography," Measur. Sci. Tech. **10**, 1142 (1999).
[19] S. M. Gallager, H. Yamazaki, and C. S. Davis, "Contribution of fine-scale vertical structure and swimming behavior to formation of plankton layers on georges bank," Mar. Ecol. Prog. Ser. **267**, 27 (2004).
[20] L. T. Mouritsen and K. Richardson, "Vertical microscale patchiness in nano-and microplankton distributions in a stratified estuary," J. Plank. Res. **25**, 783 (2003).
[21] M. M. Dekshenieks, P. L. Donaghay, J. M. Sullivan, J. Rines, T. R. Osborn, and M. S. Twardowski, "Temporal and spatial occurrence of thin phytoplankton layers in relation to physical processes," Mar. Ecol. Prog. Ser. **223**, 61 (2001).
[22] O. M. Cheriton, M. A. McManus, D. V. Holliday, C. F. Greenlaw, P. L. Donaghay, and T. J. Cowles, "Effects of mesoscale physical processes on thin zooplankton layers at four sites along the west coast of the us," Estuaries Coasts **30**, 575 (2007).
[23] J. H. Churnside and P. L. Donaghay, "Thin scattering layers observed by airborne lidar," ICES J. Mar. Sci. **66**, 778 (2009).

[24] J. V. Steinbuck, M. T. Stacey, M. A. McManus, O. M. Cheriton, and J. P. Ryan, "Observations of turbulent mixing in a phytoplankton thin layer: Implications for formation, maintenance, and breakdown," Limn. Ocean. **54**, 1353 (2009).
[25] W. M. Durham and R. Stocker, "Thin phytoplankton layers: Characteristics, mechanisms, and consequences," Annu. Rev. Mar. Sci. **4**, 177 (2012).
[26] M. S. Hoecker-Martínez and W. D. Smyth, "Trapping of gyrotactic organisms in an unstable shear layer," Cont. Shelf Res. **36**, 8 (2012).
[27] Z. Wang and L. Goodman, "The evolution of a thin phytoplankton layer in strong turbulence," Cont. Shelf Res. **30**, 104 (2010).
[28] J. M. Sullivan, M. A. McManus, O. M. Cheriton, K. J. Benoit-Bird, L. Goodman, Z. Wang, J. P. Ryan, M. Stacey, D. Van Holliday, C. Greenlaw, M. A. Moline, and M. McFarland, "Layered organization in the coastal ocean: An introduction to planktonic thin layers and the loco project," Cont. Shelf Res. **30**, 1 (2010).
[29] G. I. Sivashinsky, "Weak turbulence in periodic flows," Physica D **17**, 243 (1985).
[30] Z. S. She, "Metastability and vortex pairing in the kolmogorov flow," Phys. Lett. A **124**, 161 (1987).
[31] V. Borue and S. A. Orszag, "Numerical study of three-dimensional kolmogorov flow at high reynolds numbers," J. Fluid Mech. **306**, 293 (1996).
[32] S. O'Malley and M. A. Bees, "The orientation of swimming biflagellates in shear flows," Bull. Mathe. Biol. **74**, 232 (2012).
[33] S. A. Thorpe, *An Introduction to Ocean Turbulence* (Cambridge University Press, 2007).
[34] S. Musacchio and G. Boffetta, "Turbulent channel without boundaries: The periodic kolmogorov flow," Phys. Rev. E **89**, 023004 (2014).
[35] G. Bluman and S. C. Anco, *Symmetry and Integration Methods for Differential Equations* (Springer, 2002), Vol. 154.
[36] I. A. García and M. Grau, "A survey on the inverse integrating factor," Qual. Th. Dyn. Syst. **9**, 115 (2010).
[37] A. J. Lichtenberg and M. A. Lieberman, *Regular and Chaotic Dynamics* (Springer, 1992).
[38] P. G. Harper, "The general motion of conduction electrons in a uniform magnetic field, with application to the diamagnetism of metals," Proc. Phys. Soc. Sec. A **68**, 879 (1955).
[39] M. A. Bees, N. A. Hill, and T. J. Pedley, "Analytical approximations for the orientation distribution of small dipolar particles in steady shear flows," J. Math. Biol. **36**, 269 (1998).
[40] N. A. Hill and D. P. Häder, "A biased random walk model for the trajectories of swimming micro-organisms," J. Theor. Biol. **186**, 503 (1997).
[41] V. A. Vladimirov, T. J. Pedley, P. V. Denissenko, and S. G. Zakhidova, "Measurement of cell velocity distributions in populations of motile algae," J. Exper. Biol. **207**, 1203 (2004).
[42] M. Polin, I. Tuval, K. Drescher, J. P. Gollub, and R. E. Goldstein, "Chlamydomonas swims with two "gears" in a eukaryotic version of run-and-tumble locomotion," Science **325**, 487 (2009).
[43] S. Redner, *A Guide to First Passage Processes* (Cambridge University Press, 2001).
[44] M. Sandoval, N. K. Marath, G. Subramanian, and E. Lauga, "Stochastic dynamics of active swimmers in linear flows," J. Fluid Mech. **742**, 50 (2014).